Available online at www.sciencedirect.com

ScienceDirect

Journal of the European Ceramic Society 35 (2015) 1725–1736

www.elsevier.com/locate/jeurceramsoc

Contact damage of silicon carbide ceramics with different grain structures measured by Hertzian and Vickers indentation☆

James Wade, Santonu Ghosh, Phoebe Claydon, Houzheng Wu *

Department of Materials, Loughborough University, Leicestershire LE11 3TU, UK

Received 4 August 2014; received in revised form 5 December 2014; accepted 26 December 2014
Available online 9 January 2015

Abstract

We have used Hertzian and Vickers indentation to investigate contact damage in sintered SiC ceramics, one consisting of uniform, fine-grains and the other a coarse, elongated grain structure. Cracking-resistance measured by Hertzian indentation, showed no discernible difference, nor did the Vickers hardness. However, numerical analysis of the Vickers indentation size effect, performed using the proportional specimen resistance model, indicates 77.3% greater surface energy, mostly realised through cracking, is experienced by heterogeneous SiC per unit area of indentation impression. This is typified by an observable increase in the number of radial cracks generated around Vickers impressions, which has been found to artificially increase the K_{IC} determined by Vickers indentation fracture. Quantitative measurements of pre-existing flaws by Hertzian indentation show that heterogeneous SiC retains a higher density of larger flaws. Relationships between the differences in cracking around Vickers indents and the pre-existing flaw populations of these two SiC ceramics are discussed.

Keywords: Cracking-resistance; Flaw density; Grain structure; Porosity; SiC

1. Introduction

Silicon carbide (SiC) ceramics have been increasingly used as structural materials designed to endure a wide range of static/dynamic contact loads, particularly as part of composite armour or as bearings, gaskets and other wear components, largely because of their high hardness, outstanding damage tolerance and low density. Conventionally, for such applications, hot-pressed SiC would be the favoured material. Nevertheless, sintered SiC is more economical to manufacture, a fact that is well-considered in its commercial use. Unfortunately though, the microstructures of sintered SiC can be susceptible to large variations in grain size and shape, especially if the dwell period or the peak sintering temperature has not been optimised.[1–3] This is because, in order to promote the dissolution–precipitation mechanism of material transportation needed to achieve full densification, sintering is usually assisted by a vitreous phase.[4,5] As such, sintered SiC ceramics can have a homogeneous or heterogeneous grain structure, also commonly referred to as unimodal or bimodal/multimodal respectively.[2,3] It is inevitable that with such abnormal grain growth we see a transformation in the microstructural features, namely pore size and flaw distributions. However, to date, little work has been done on understanding how such changes influence the resistance to contact damage in ceramics.

It is generally acknowledged that a measurement of contact damage should include aspects of both plastic deformation and brittle fracture. Thus, contact damage in ceramics is widely imitated by Vickers indentation, where, for most ceramics, lattice flow and cracking happen simultaneously around the indentations generated, even at low loads.[6,7] For some researchers, the fracturing that occurs during such tests is thought to result in the well-established indentation size effect (ISE) i.e. a drop in hardness with increasing load. Recently, Li and Bradt proposed a proportional specimen resistance (PSR) model,[8] where the contributions of cracking and permanent deformation to the

☆ Research data for this paper is available on request from Dr Houzheng Wu via email (h.wu2@lboro.ac.uk)

* Corresponding author. Tel.: +44 1509 223342; fax: +44 1509 223949.
E-mail address: h.wu2@lboro.ac.uk (H. Wu).

http://dx.doi.org/10.1016/j.jeurceramsoc.2014.12.030

total work imparted during indentation can be resolved into two individual values by fitting the Vickers indentation data taken across a range of loads that clearly show an ISE. By adopting the PSR model, we comparatively evaluate the amount of cracking and plastic deformation experienced by sintered homogeneous and heterogeneous SiC and are able to quantitatively assess the contact damage resistance of each grain structure.

For the polycrystalline ceramics used in this study, the resistance of lattice flow can differ due to a grain boundary affect, which can constrain the movement of dislocations based on the Hall–Petch model.[9] As for the cracking damage, following the principles of fracture mechanics, this is governed by the fracture toughness/critical stress intensity factor (K_C) and the size of pre-existing flaws/defects. Hence, in this study, we also quantitatively measure the flaw populations of homogeneous and heterogeneous SiC using Hertzian indentation, a method proposed by Warren[10], as well as the K_C.

For ceramics, the most measured K_C is that under tension, referred to as mode I or K_{IC}. Given its importance, a range of experimental methods have been developed in order to accurately measure such a property. One category is based on bending specimens with pre-developed cracks, such as single-edge notched beam (SENB), single-edge pre-cracked beam (SEPB), single-edge V-notched beam (SEVNB), chevron-notch (CN) and double cantilever beam (DCB). All of these can give a clearly defined type I, pure tensile stressing condition and, presumably, single crack propagation. Nevertheless, the measurements have a strong dependency on the geometric configuration of the notches or pre-cracks, which are unlikely to be kept the same from one laboratory to another due to the constraint of local capability and expertise in machining. Another category is based on simple indentation techniques i.e. Vickers indentation fracture (VIF) and Hertzian indentation. These are probably the most convenient testing methods as the sample preparation requirements are minimal, the tests are performed on standardised equipment and there are no sample size issues to consider. Of the two indentation based methods, VIF is certainly the most popular and has been readily used to resolve the K_{IC} of sintered SiC ceramics, as well as many others.[2,3,11,12] However, in recent years, the measurements of K_{IC} by VIF have been recently questioned by Morrel, Quinn and Bradt, owing to the poor definition of the type I stress responsible for crack initiation and propagation.[13,14] Quinn and Bradt made a strong argument that "*VIF does appear to represent some form of a complex crack arrest phenomenon*" and, consequently, they have called for an end in its use in the measurement of K_{IC}. Alternatively, unlike Vickers, Hertzian indentation, which was first instrumented to measure K_{IC} by Warren almost two decades ago,[15] relies on pre-existing surface flaws, introduced by the surface finish and/or borne inherently, with a high enough density to be activated inside a well-defined tensile stress field near the boundary of Hertzian contact. When the load necessary for the initiation of a typical ring-crack is captured, only a single crack propagates without plastic deformation and/or any form of crack suppression, providing a more precise account of the K_{IC}. On this basis, we utilise Hertzian indentation to determine the K_{IC} of SiC with a homogeneous and heterogeneous grain structure. At the same time, measurements achieved by using VIF will be investigated to evaluate Quinn and Bradt's assertion on crack arrest by using indentation-based numerical modelling and observational analysis of crack paths generated by Vickers indentation.

2. Experimental procedure

2.1. Materials

Two commercial samples of monolithic α-SiC ceramics were supplied by Morgan AM&T (Swansea, UK). All samples were die-pressed from the same starting powders and sintered in a vacuum furnace at a temperature of around 1900 °C. In order to achieve SiC ceramics of varied grain sizes and morphology, this was followed by a post-sintering annealing process at ∼2000 °C over selected dwell periods. In general, ceramics that remain unexposed to such a heat treatment will maintain smaller grains of an equiaxial form, usually labelled as either unimodal or homogenous SiC (herein coded as U-SiC); a prolonged dwelling time promotes abnormal grain growth leading to larger grains of an elongated or plate-like shape, commonly referred to as heterogeneous or bimodal SiC (herein coded as H-SiC). The as-received samples included one type of unimodal and several types of heterogeneous SiC each differentiated by the volume fraction, size and aspect ratio of the elongated grains. Any density measurements were made using the Archimedes method.

2.2. Sample preparation

The as-received SiC square tiles, with a measured edge length of ∼100 mm and a thickness of ∼8.5 mm, were cut using a diamond saw into small sections. Each sample was then mounted onto a flat mild steel block and lapped on a bench mounted KEMET 15 flat-bed diamond lapping machine (Kemet International, Maidstone, UK). Diamond slurries of 25 μm, 8 μm were used in conjunction with a hard plate whilst a soft cloth was used for polishing at 3 μm and 1 μm. Each step of the lapping/polishing sequence was selected to remove all surface damage introduced by the previous step and carried out until a smooth, high-shine 1 μm surface-finish was accomplished.

A selection of samples were chemically etched to expose the microstructure by introducing them to a modified Murakami's reagent containing 3 g of potassium hydroxide (≥85% KOH), 30 g of 99% pure potassium ferricyanide ($K_3Fe(CN)_6$) and 60 ml of distilled water. The polished samples were submerged in the boiling solution for 20–25 min until a satisfactory etch was achieved. FEG-SEM images of the resolved microstructures were then taken in a Carl Zeiss (Leo) 1530 VP scanning electron microscope (Carl Zeiss, Cambridge, UK) under an accelerating voltage of 5.00 kV.

2.3. Measurements of grain and porosity populations

Planar measurements of grain size were made using the intercept method by superimposing an evenly spaced grid of test lines

over SEM images of etched samples and estimating the distance between the points at which the grain boundary intersected the grid, known as the intercept length. Due to the millimetre- to micron-sized grain distribution in the H-SiC, this method was practiced 5 times on SEM images taken at 150–900× magnification. At low magnification, grains deemed too small for measurement were overlooked, but remain accounted for at higher magnifications.

As for the porosity measurements, these were made by manually measuring the maximum diameter or length of pores that appeared on the fracture surface of a sample. For statistical reliability, this was done over 1000× across multiple SEM images.

2.4. Vickers indentation and interpretation of indentation measurements

Two Vickers indenters were employed to produce indents; a Mitutoyo HM-124 (Mitutoyo UK Ltd, Andover, UK) at loads of 0.05–2 kgf (0.49–19.61 N) and an Innovatest Nexus 4503 (Innovatest Europe, Maastricht, The Netherlands) for higher loads of 2.5–10 kgf (24.51–98.07 N).

For determining the hardness, at least 5 indents were made at each load and comprised of minimal crack formations, voids and any other features which may inhibit their precise dimensional assessment. All tests were performed with a 15-s holding time and at room temperature. The resultant indents were imaged in the SEM and measured using graphic editing software (Adobe Photoshop, USA). The hardness (H) was calculated using following equation:

$$H = \alpha \frac{P}{d^2} \tag{1}$$

where d is an average of the respective horizontal and vertical diagonal length for each indent in μms, α is a constant contingent on the indenter shape with a value of 1.8544 for a Vickers profile, and P is indentation load in Newtons. Given that hardness measurements were made over a range of loads, the extent of each ISE can be quantified by calculating the exponent, n, as defined by Meyer's Law[16]:

$$P = Ad^n \tag{2}$$

where regression analysis can be employed to acquire the A and n constants. In the absence of an ISE, $n = 2$; any deviation below this value may act as an inverse indicator of the ISE severity. The hardness measurements were also fit by the PSR model of Li and Bradt[8]:

$$P = a_1 d + a_2 d^2 \tag{3}$$

Here, the load-dependent ISE is deconvolved into two individual terms, factored by a_1 and a_2 respectively. It is generally acknowledged that the a_2 denotes the resistance to crack-free plastic deformation, i.e. lattice flow, and can be used to estimate the load-independent hardness based on the indenter profile. Conversely, the a_1 term is believed to relate to the degree of cracking introduced by indentation.[6,17,18]

Vickers indentation fracture (VIF) toughness measurements, made over a load range of 0.3–10 kgf, were calculated using the equation of Anstis et al.[19]:

$$K_{IC} = 0.016\left(\frac{E}{H}\right)^{1/2} \times \frac{P}{c^{3/2}} \tag{4}$$

where E is the Young's modulus, H is the hardness in GPa and c is the total distance from the centre of the impression to the radial crack tip in μms.

In order to examine the crack path interactions between the contrasting grain structures of U-SiC and H-SiC, 10 kgf Vickers indents were generated on the surface of chemical etched samples. Observations of the radial crack patterns emanating from the corners of the indentation impressions were then made in the SEM.

2.5. Hertzian indentation and flaw population measurements

Hertzian indentation tests were carried out using a CK10 testing machine (Engineering Systems, Nottingham, UK) fitted with a wide-band acoustic emission transducer at a frequency of 90 kHz to detect the loading point at which characteristic Hertzian ring-cracks initiated on the surface.

A series of tests were performed on the 1 μm polished surfaces of U-SiC and H-SiC using spherical indenters of 1.5 mm, 2.5 mm and 5 mm radiuses. In this experiment, all indenters and the indented substrates were composed of pressureless-sintered SiC. Since the elastic properties of the indenter and the indented materials are identical, the contributions of friction at the contact interface have been ignored in the following calculations.

The Hertzian indentation tests involved measuring, over a range of indents (~25), the minimum load (P_{min}) at which the aforementioned Hertzian cracks initiate and the size of the resultant ring-crack. The cumulative probability of ring-crack generation with increasing load during Hertzian indentation for each specimen was determined by:

$$P_n = \frac{n}{N+1} \tag{5}$$

where n is the order number of each data point once the cracking loads (P_n) have been arranged in ascending order and N is the total number of data recorded.

In accordance with Warren,[15] the K_{IC} can be attained using the following equation:

$$K_{IC} = \sqrt{\frac{E * P_{min}}{P_{FN}^{min} R}} \tag{6}$$

where P_{FN}^{min} is a dimensionless constant that depends solely on the Poisson's ratio, ν, of the tested material. For SiC, this is assumed to be 0.17, corresponding to P_{FN}^{min} value of 1386, as tabulated by Warren.[15] The ball radius is denoted as R, and E^* is determined by:

$$\frac{1}{E*} = 2 \times \frac{1-\nu^2}{E} \tag{7}$$

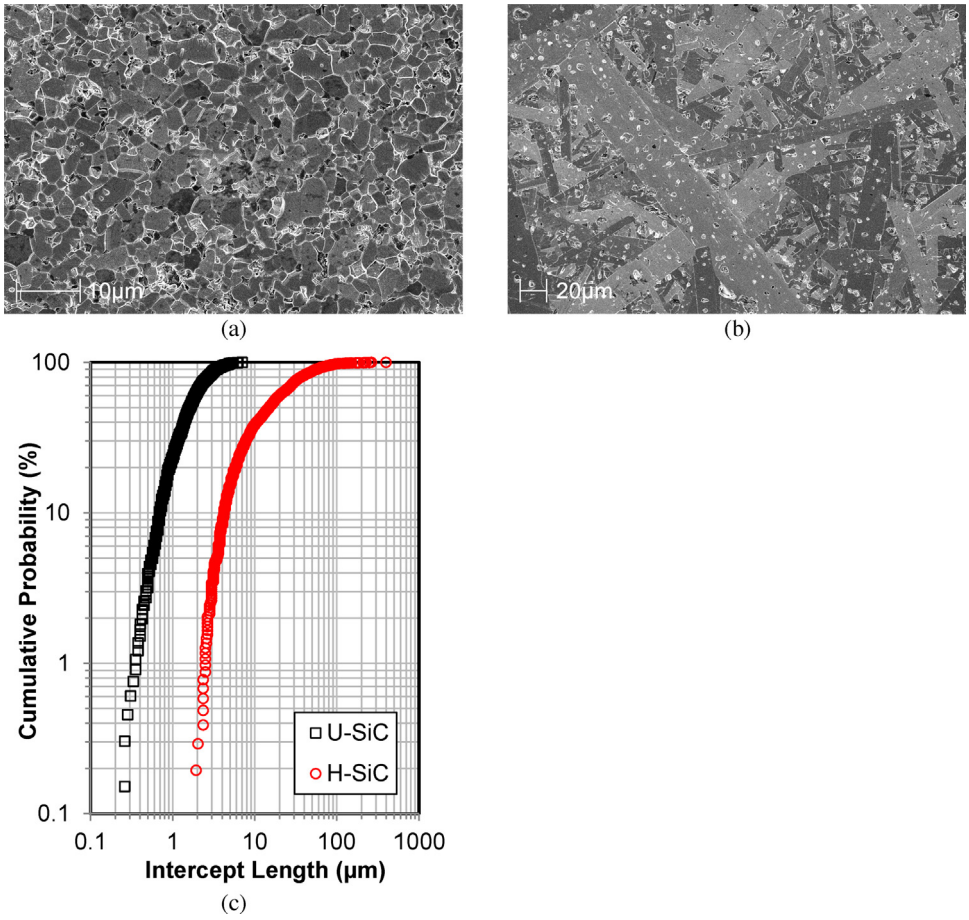

Fig. 1. FEGSEM (Inlens) images of as-received SiC microstructures after 1 μm polishing and chemical etching: (a) U-SiC consists of an equiaxed, fine-grain structure; (b) H-SiC exhibits coarse, elongated grains; (c) the cumulative probability of intercept lengths measured in SiC ceramics using meshed method.

With the experimentally measured P_{min} and ring-crack diameters, the size and density of surface flaws, assumed to be a half-penny shape perpendicular to the surface and parallel with the radial direction of their normals, can be estimated as follows.

By understanding that a ring-crack with a diameter of r_i is generated under an indenting load of P_i, the flaw size (c_i) can be calculated using the equation below:

$$c_i = \left(\frac{2\pi}{Y(1-2\nu)} \times K_{IC} \times \frac{r_i^2}{P_i} \right)^2 \tag{8}$$

where Y is a geometric factor approximately equal to 0.713.

Consequently, the total area searched, $A(P_i,c_i)$, in loading up to P_i is defined by:

$$A(P_i, c_i) = \pi(r_{max}^2 - r_{min}^2) \tag{9}$$

here, r_{max} and r_{min} are the maximum and minimum distance at which a flaw, with a size larger than c_i, may be detected away from the centre of the Hertzian contact region. The r_{max} and r_{min} can be estimated using Eqs. (10a) and (10b), respectively:

$$r_{max} = \left(\frac{Y(1-2\nu)P\sqrt{c}}{2\sqrt{\pi}K_{IC}} \right)^{1/2} \tag{10a}$$

$$r_{min} = \frac{3\sqrt{\pi}RK_{IC}}{2Y(1-2\nu)E^*c^{1/2}} \tag{10b}$$

Note, the power of c in equation 13e in Warren's paper[10] is incorrect (credited to the reviewer of this paper). The estimated flaw density for cracks at a length equivalent to c_i is the reverse of the searched area by the indenter:

$$\rho(c_i) = \frac{1}{A(P_i, c_i)} \tag{11}$$

3. Experimental results and discussion

3.1. Grain structure measurements

The microstructures of U-SiC and H-SiC are displayed in Fig. 1(a) and (b), respectively. A comparison of the two samples highlights an apparent transition from fine, equiaxed grains to a coarser, elongated or plate-shaped grain structure. The degree of grain heterogeneity has been quantified by manually measuring the aspect ratios of each grain, and the intercept lengths of grain boundaries within a defined grid, as presented in Fig. 1(c). For U-SiC, an average aspect ratio of 1.44 ± 0.38 suggests an almost equiaxed grain shape, whereas the H-SiC has an average aspect ratio of 9.35 ± 4.62, typical of a highly

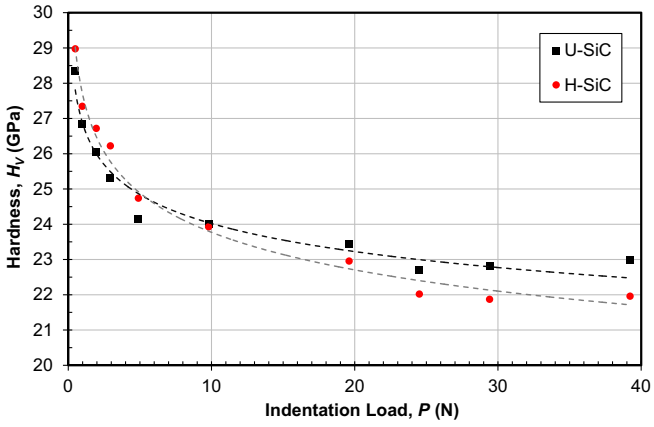

Fig. 2. Vickers hardness as a function of indentation load for U-SiC and H-SiC.

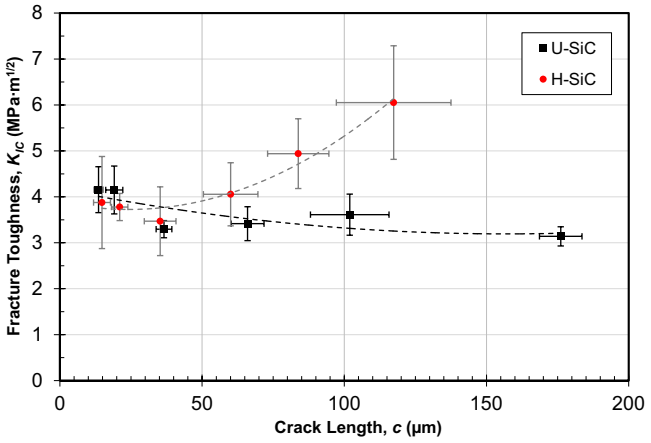

Fig. 3. The calculated Vickers indentation fracture toughness in relation to crack length for U-SiC and H-SiC.

Table 1
Vickers hardness at varying loads accompanied by uncertainties of one standard deviation.

Load (N)	U-SiC H_V (GPa)	H-SiC H_V (GPa)
0.49	28.34 ± 0.8	28.97 ± 1.4
0.98	26.83 ± 0.8	27.34 ± 0.5
1.96	26.05 ± 0.8	26.72 ± 0.5
2.94	25.31 ± 0.5	26.22 ± 1.6
4.91	24.14 ± 2.4	24.74 ± 1.2
9.81	24.02 ± 1.0	23.93 ± 0.9
19.62	23.44 ± 1.5	22.95 ± 0.6
24.53	22.71 ± 0.5	22.02 ± 0.8
29.43	22.80 ± 0.2	21.87 ± 0.6
39.24	22.99 ± 0.3	21.96 ± 1.1

elongated or heterogeneous grain morphology. Intercept length distributions of 0.15–7 μm for U-SiC and 2–400 μm for H-SiC also indicates that an increase in grain scale coincides with such anisotropic grain growth. Note, from 2 to 7 μm, ∼40% of the U-SiC grain scale distribution overlaps with ∼30% of the H-SiC grain scale distribution.

3.2. Vickers Hardness and the indentation size effect

The Vickers hardness values (H_V) for U-SiC and H-SiC, determined in accordance with Eq. (1), are graphically depicted as a set of hardness-load curves in Fig. 2. Here each of the plotted data points is the average of 5 indent measurements. For clarity and conciseness, all error bars of one standard deviation have been omitted and are, in preference, presented as confidence intervals in Table 1.

Overall, the H_V statistics attained, whilst at the lower-limit, are within the boundaries of what is to be expected for SiC. Fig. 2 shows, across a low load-regime, both ceramics exhibit a marked decrease in the H_V with increasing load, validating the presence of an ISE, and follow a relatively similar non-linear trend, eventually diverging at a higher load range of ∼10–40 N. Close examination of the data over this plateaued-region consistently demonstrates that U-SiC possesses a slightly higher H_V (∼23 GPa) over H-SiC (∼22 GPa).

By employing Meyer's law,[16] the extent of each ISE can be quantified by the value of exponent, n, defined in Eq. (2). As expressed in Table 2, n values of <2 confirm that both SiC ceramics experience an ISE. In addition, H-SiC, with a lower n, suffers from a heightened ISE.

The PSR modelling results, also presented in Table 2, show that U-SiC has a higher load-independent hardness (H_{PSR}) compared to H-SiC. Such a trend, together with the ∼3% (0.72 GPa) difference in hardness, is well-aligned with the experimentally derived H_V data. We suspect such variations are most likely governed by the smaller microstructural grain size of U-SiC, a phenomenon originally professed by Rice.[9] In any event, the contributions of grain size to the overall hardness appears to be marginal, especially given that significant dissimilarities between the intercept lengths of U-SiC and H-SiC, shown in Fig. 1(d), do not correlate with the moderate difference in hardness. This demonstrates that the resistance to contact damage by plastic deformation is essentially identical in these two samples.

Therefore, of greater interest is the a_1, which exhibits a considerably more substantial increase from U-SiC to H-SiC. This

Table 2
A summary of the n and A parameters determined using the Meyer's Law together with the a_1, a_2 terms according to the PSR model and load-independent hardness values.

Materials	Meyer's law		Proportional specimen resistance model		
	n	A	a_1	a_2	H_{PSR} (GPa)
U-SiC	1.907	52.85	22.08 ± 7.3	11,918.57 ± 157	22.10
H-SiC	1.876	50.16	39.15 ± 4.5	11,532.0 ± 974	21.38

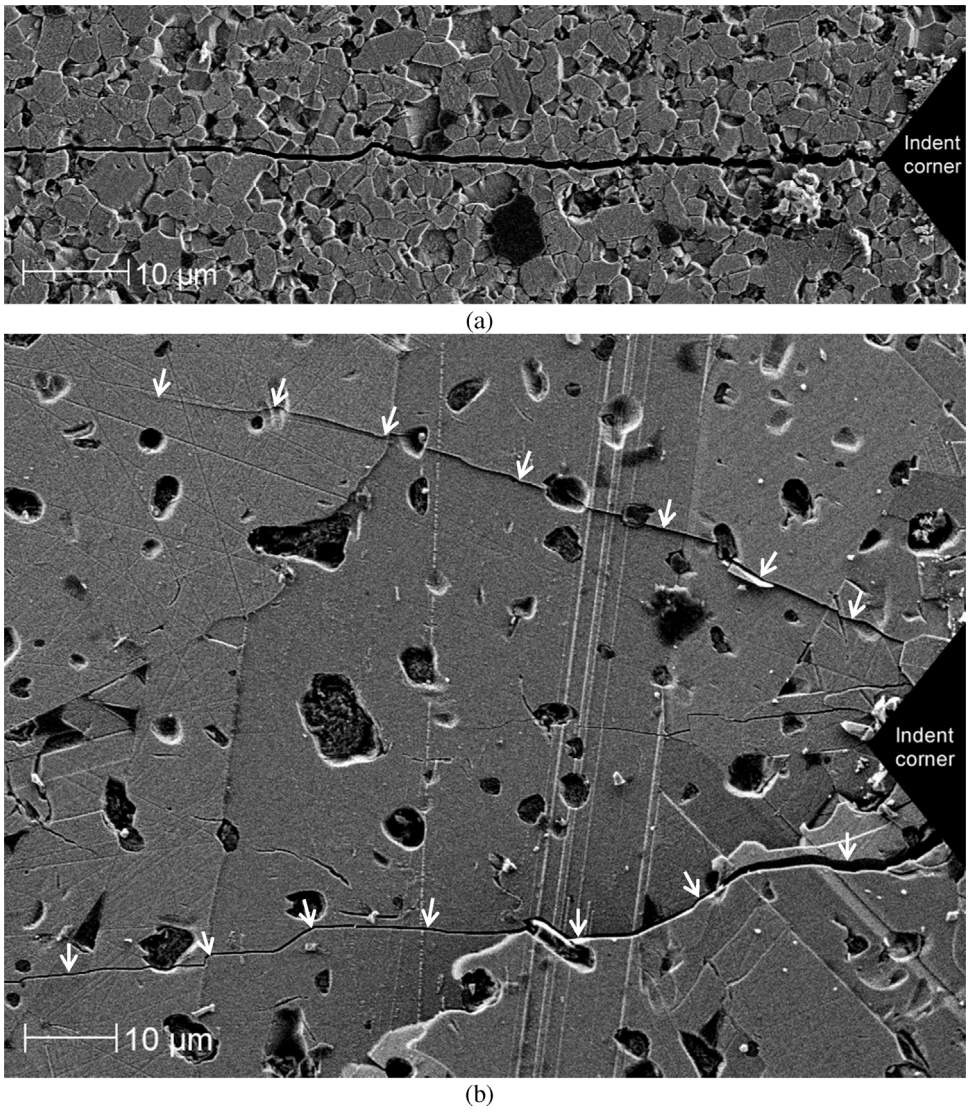

Fig. 4. Classic radial cracking on as-received SiC specimens after 1 μm polishing and chemical etching: (a) U-SiC, composed of straight, clean, transgranular crack extensions and (b) H-SiC produced more intricate transgranular crack paths with multiple non-diagonal radial cracks (as arrowed) forming in close proximity to the corner cracks.

implies that the a_1 holds more significance in regards to the total performance of these sintered SiC ceramics under external loading. If one accepts Quinn and Quinn's analysis[18] that the a_1 accounts for the effects imposed by the ISE and that the ISE is caused by the crack formations underneath and around the indentation impression, larger a_1 values indicate proportionally greater contact damage through cracking.

As mentioned previously, linear fracture mechanics dictates that the cracking initiation and propagation that occurs here is governed by the stress intensity factor (K) that is determined by the size of pre-existing flaws and stress field around their tips. When the K is larger than the critical stress intensity factor (K_C), cracking is triggered, followed by further propagation until K declines to a level below the K_C. Therefore, one must determine the fracture toughness in order to be assured that the difference in the calculated contact damage by means of cracking is not influenced by changes in the K_{IC} of each grain structure, as lower values may facilitate easier crack initiation and propagation. As already stated, traditionally, the method used to differentiate the K_{IC} in homogeneous and heterogeneous ceramics has been VIF. Therefore, we also performed VIF to determine the K_{IC}. However, this has been done in order to show that, be it real or superficial, there is what could be argued as a "toughening" effect in the heterogeneous ceramic material presented herein, and not as an appropriate means of determining the K_{IC}. For this we have used a much more reliable method, Hertzian indentation. The results of both tests are discussed below.

3.3. Fracture toughness measured by Vickers indentation

Fig. 3 displays the fracture toughness values resolved using the VIF method. Here, U-SiC undergoes a minor reduction in the calculated K_{IC} with an enlarging crack size from 4.16 MPa $m^{1/2}$ to 3.14 MPa $m^{1/2}$. Results show that measurements of lower value experience long crack propagation, meaning U-SiC seems to encounter a form of inhibited crack growth at lower loads. A

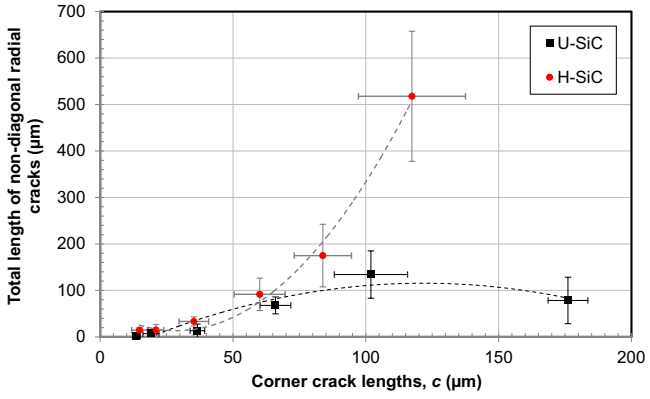

Fig. 5. The total length of non-diagonal radial cracks generated in U-SiC and H-SiC by Vickers indentation at 0.3–10 kgf against the measured corner crack length, c, used to determine the VIF cracking-resistance.

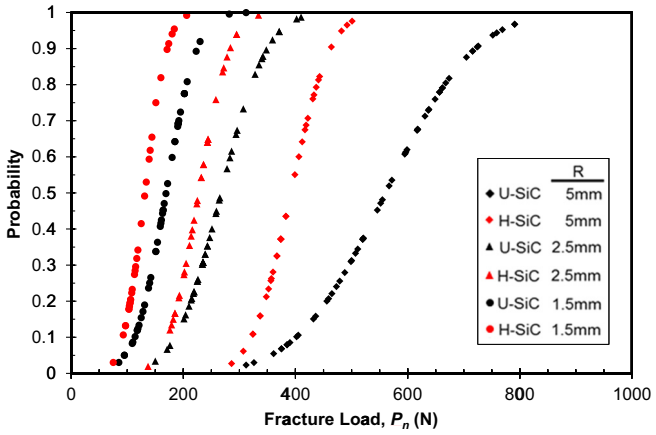

Fig. 6. The cumulative probability of ring-crack generation during Hertzian indentation with spherical indenters of varying radiuses 1.5, 3 and 5 mm for U-SiC (black symbols) and H-SiC (red symbols).

probable cause could be the complex and interacting compressive stress field near the elastic/plastic boundary and directly behind the propagating crack, the effects of which become proportionally less as the crack extends farther into the elastic field. Consequently, the apparent crack propagation resistance drops to a value closer to that of a pure tensile stressing condition. Micrographical inspection of radial crack patterns produced during VIF at 10 kgf confirms that U-SiC experiences pure transgranular fracture, as illustrated in Fig. 4(a). This is further supported by the generation of a smooth fracture surface, indicating no change in fracture mode with crack growth. As predicted, qualitative analysis of crack path interactions with the microstructure of U-SiC did not yield any signs of crack-bridging.

In contrast, the K_{IC} values for H-SiC, derived using VIF method, show a steady increase in the crack-growth resistance over ~120 μm of crack extension, from an initial K_{IC} equalling 3.88 MPa $m^{1/2}$ up to a maximum K_{IC} value of 6.05 MPa $m^{1/2}$, an improvement of ~56%. This characteristic "R-curve behaviour" is thought to be emblematic of a typically heterogeneous microstructure and has been attributed to the crack-bridging that occurs behind the propagating crack and/or crack-deflection that appears in the front of the crack tip,[20,21] the effects of both becoming more conducive to the K_{IC} with further crack development. However, in radial crack patterns produced during VIF at 10 kgf, exemplified in Fig. 4(b), H-SiC primarily exhibits transgranular fracture and, more importantly, shows no obvious indications of the crack-bridging/deflection mechanisms necessary to achieve such an R-curve in heterogeneous SiC. Such findings are of particular interest as they are inconsistent with the original work performed by Padture and Lawn,[21] where observations on heterogeneous silicon carbide revealed deflected cracking along grain boundaries and extensive crack-bridging. However, differences in the sample compositions are particularly important to note. In the Padture and Lawn's samples, large quantities of sintering aids were used to induce the heterogeneous microstructure through liquid-phase sintering. These additives then coalesced at the grain interface to form "*a residual intergranular second phase – yttrium aluminium garnet (YAG) crystalline*". This YAG phase gives a difference in the coefficient of thermal expansion (CTE) of 5×10^{-6}, leading to substantial residual stresses at the interface boundaries. It is these residual stresses that cause the de-bonding along the grain boundaries of the elongated/large grains in the SiC ceramic with a heterogeneous grain structure, resulting in a distinct fracture morphology consistent with that of intergranular fracture, which, as shown in Figs. 1 and 2 in their paper, included grain-bridging and pull-out linked to the elongated grains. Conversely, because the heterogeneous microstructure of H-SiC has been induced through a post-sintering annealing process, rather than by introducing larger quantities of additives, there is little change in the residual stresses between the interface phase and the SiC grains, meaning the strength of the grain boundary in H-SiC should be closer to that of homogeneous SiC. Therefore, it is not unreasonable to suggest that crack-bridging does not take place in H-SiC and/or its effectiveness is negligible due to the lack of a weak grain boundary. Consequently, we question the "R-curve behaviour" shown in Fig. 3, but are curious to know the potential contributor to this behaviour if not due to crack-bridging. To this end, in closely examining of the Vickers indents used for VIF in H-SiC, instead of cracking-bridging, we repeatedly recorded numerous radial cracks emanating from locations other than the corners of the indent, herein referred to as cracks of a non-diagonal direction, some of which are arrowed in Fig. 4(b). From Fig. 4(a) it is obvious that such radial cracks of a non-diagonal direction are infrequent in U-SiC. This was consistent across the entire indentation load regime and consistent with the a_1 values for cracking damage derived for each sintered SiC grain structure. Estimates for the total length of non-diagonal radial cracks are plotted in Fig. 5 against corner crack length, c, from Eq. (4). For U-SiC, only a limited relationship exists between the development of additional non-diagonal radial cracks and corner crack propagation. Yet the featured curve of H-SiC displays an appreciable increase in the total non-diagonal radial crack length with an enlarging corner crack, a trend akin to that of its K_{IC} with crack extension. Therefore, we conclude that, in H-SiC, the extent to which each corner crack propagates may be constrained by the nucleation and growth of the non-diagonal radial

Table 3
The minimum loads, ring-crack diameters, estimated flaw size for ring crack initiation and fracture toughness values of U-SiC and H-SiC at each spherical indenter ball size.

Material	Ball indenter radius (mm)	P_{min} (N)	Ring-crack diameter (μm)	Flaw size for ring-crack initiation based on P_{min}	K_{IC} (MPa m$^{1/2}$)
U-SiC	1.5	72	181.8	6.6	2.83
	2.5	145	216.6	3.3	3.11
	5	312	431.3	11.2	3.23
H-SiC	1.5	69	179.3	6.8	2.77
	2.5	130	227.3	5.0	2.95
	5	290	342.1	5.1	3.11

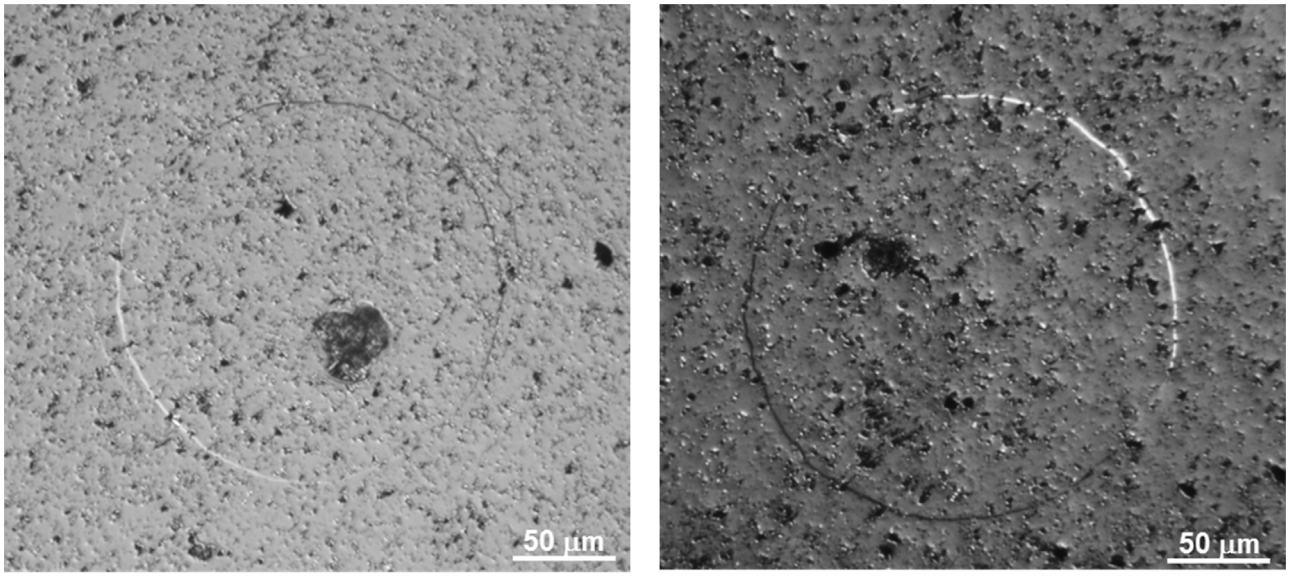

Fig. 7. Hertzian ring-cracks generated on a well-polished surface of (a) U-SiC and (b) H-SiC with SiC spheres of 2.5 mm in radius.

cracks i.e. greater cracking damage, which are not considered in the analysis of VIF. Of course, the generation of the multiple subsidiary cracks which appear in the vicinity of primary cracks, as shown in Fig. 4(b), may also assist in establishing a high K_{IC}, but we surmise this to be of relative insignificance given the small quantities and crack lengths observed.

Combining the observations in Fig. 4(a) and (b) with the measurements made in Fig. 5 conclusively demonstrates that, for H-SiC, the seeming improvement in cracking-resistance with increasing corner crack size may not be caused by a change in the real K_{IC}, but presumably by the multiplication of non-diagonal radial cracks about the indentation impression. At present, we are unsure how the multiplication mechanism inhibits the propagation of corner cracks. In order to uncover such details, further systematic evaluation is necessary, but this certainly affirms Quinn and Bradt's concerns in using this method to measure such a property.

3.4. Fracture toughness measured by Hertzian indentation

Having considered the potentially misleading nature and/or the unreliability of the data produced by VIF, Hertzian indentation tests were performed, the results of which are portrayed in Fig. 6 as a fracture probability against load diagram. Importantly, the minimum fracture loads for both specimens are a true asymptote and, thus, can be used with confidence to determine the K_{IC}. The calculated fracture toughness values are tabulated in Table 3 along with the measured ring-crack diameters and estimated sizes of pre-existing flaws responsible for the formation of such ring-cracks. Here, interestingly, U-SiC and H-SiC show only a slight variation in K_{IC} when detected by the same spherical indenter size. It is worth emphasising at this point, that, unlike VIF, Hertzian fracture, in either sample, suffers from no such multiplication mechanism, nor does it induce any form of crack-bridging or crack deflection, as illustrated by the rink-crack paths in Fig. 7 on the polished surfaces of U-SiC and H-SiC. Therefore, based on these results, we deduce that the in situ-heterogeneous microstructure developed in H-SiC has a negligible effect on the fracture toughness measured by Hertzian indentation. Although there is a tendency for the absolute values of K_{IC} to increase with an enlarged spherical indenter size, the total increment is no more than 0.4 MPa m$^{1/2}$, comparable to testing errors which arise during K_{IC} measurements using different methods.[22,23] The ascending trend, if any, appears to have no correlation with the size of pre-existing flaws, but may be associated with the statistical distribution of flaws on the

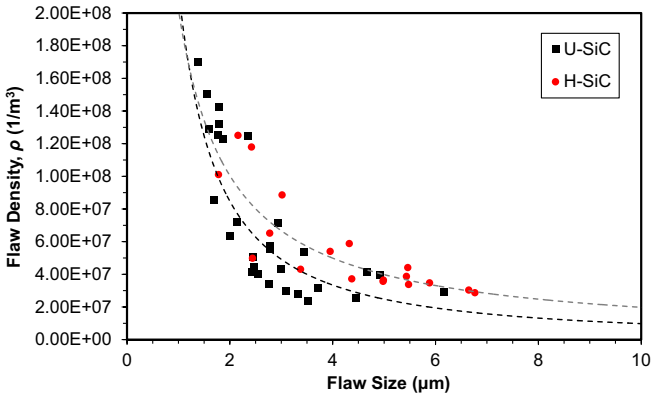

Fig. 8. Flaw populations attained using a 1.5 mm ball radius on 1 μm polished surfaces of SiC ceramics. Square and circular symbols represents U-SiC and H-SiC, respectively.

surface. It is well established that as the spherical indenter size increases, the Hertzian cracking tends to be initiated by larger pre-existing flaws. Given that our flaw size density measurements follow an inverse power function, in conducting the same number of Hertzian indentation tests, there will be a lower probability for the larger spherical indenters to have a true asymptote value close to the theoretical minimum fracture load compared to the smaller spherical indenters. This means that the estimated K_{IC} values are likely to be higher based on the minimum fracture loads measured using larger spherical indenter sizes. As can be inferred from this, if more Hertzian indentation tests were performed using the larger spherical indenter ball sizes, the statistically meaningful minimum fracture loads should be more aligned with the theoretical minimum fracture load, eliminating the increasing trends displayed by both sets K_{IC} data in Table 3.

Nevertheless, the consistency of the results exhibited by these two ceramics further suggests that the grain structure has no influence on measurements of K_{IC} and, thus, the K_{IC} has no influence in the cracking damage experienced during Vickers indentation.

3.5. Flaw population

Given the concurrent H_V, Young's modulus and K_{IC} values, one may assume that the stress configuration experienced by both sintered SiC samples to be the same. Therefore, by deduction, the ratios of a_1 should reflect the ratio of the densities of pre-existing flaws in these two SiC ceramics and, as a first approximation, have the following relationship with the size of a pre-existing flaw, c_i:

$$\frac{a_1^H}{a_1^U} = \frac{\rho(c_i)^H}{\rho(c_i)^U} \tag{12}$$

where the superscript H and U symbolise H-SiC and U-SiC respectively. To attest this correlation, it is essential to know the flaw population.

Measurements of flaw populations detected on well-polished surfaces of U-SiC and H-SiC by Hertzian indentation are presented in Fig. 8. This data set was acquired using a spherical indenter with a radius of 1.5 mm. The scattering of the measurements is likely due to statistical factors such as variations in the shape of flaws, an inevitable occurrence, and changes to the surface topography from one indentation test point to another, influencing the geometric configuration of Hertzian contact which ultimately leads to a deviation in tensile stress field from that of perfect Hertzian contact. To quantitatively assess the difference, we can fit the density of surface cracks, ρ, with an inverse power function of the detected crack size, c:

$$\rho = Ac^{-n} \tag{13}$$

where A and n are constants derived via regression analysis and displayed in Table 4. By examining the relative positions of the fitted curves in Fig. 8, it is evident that the surface of U-SiC has a higher density of smaller flaws compared to H-SiC. However, this density descends at a steeper incline, meaning U-SiC has fewer large flaws on the surface. The largest flaws detected in the heterogeneous SiC are also significantly larger than those in the homogeneous SiC, the measured density being around 10^7 m^{-2}. Flaw population measurements made using a spherical indenter with a radius of 5 mm managed to detect the largest surface flaws of ~20 μm in the U-SiC and ~40 μm in the H-SiC. Since the application depth of the radial tension immediately out of the contact boundary is proportional to the size of spherical indenter, changing the spherical indenter from a 1.5 mm to a 5 mm radius can provide an enhanced capacity to detect surface flaws which are located at deeper positions in these SiC ceramics.[24,25]

Table 4
A summary of the n and A parameters determined using the inverse power function of Eq. (13).

Sample	A		n	
	Averaged	Standard deviation	Averaged	Standard deviation
U-SiC	9.605×10^8	5.158×10^8	2.583	0.555
H-SiC	3.654×10^8	1.791×10^8	1.681	0.415

By replacing the density function of flaws in Eq. (12) with that of the measured flaw density for each SiC ceramic, the a_1 ratio is correlated to the flaw size by following expression:

$$\frac{a_1^H}{a_1^U} = 0.38c_i^{0.902} \tag{14}$$

Taken from the data listed in Table 2, the a_1 ratio of 2.11 means that pre-existing flaws larger than ~6.7 μm in size are the dominant contributors to the cracking that ensues around the indentation.

This estimation for the size of pre-existing flaws is well above the critical flaw size for the initiation of cracking and propagation. Following Lawn and Evans model,[26] they estimated a critical flaw size, c^*, as 2 μm for a hot-pressed SiC with K_{IC} value of 4 MPa m$^{1/2}$ and H_V of 19 GPa. With a lower K_{IC} measured through Hertzian cracking and marginally higher H_V measured for the U-SiC and H-SiC, the c^* is approximated to be around 1 μm.

Consequently, the calculated c_i indicates that fracture originating from pre-existing flaws with size <6.7 μm may only

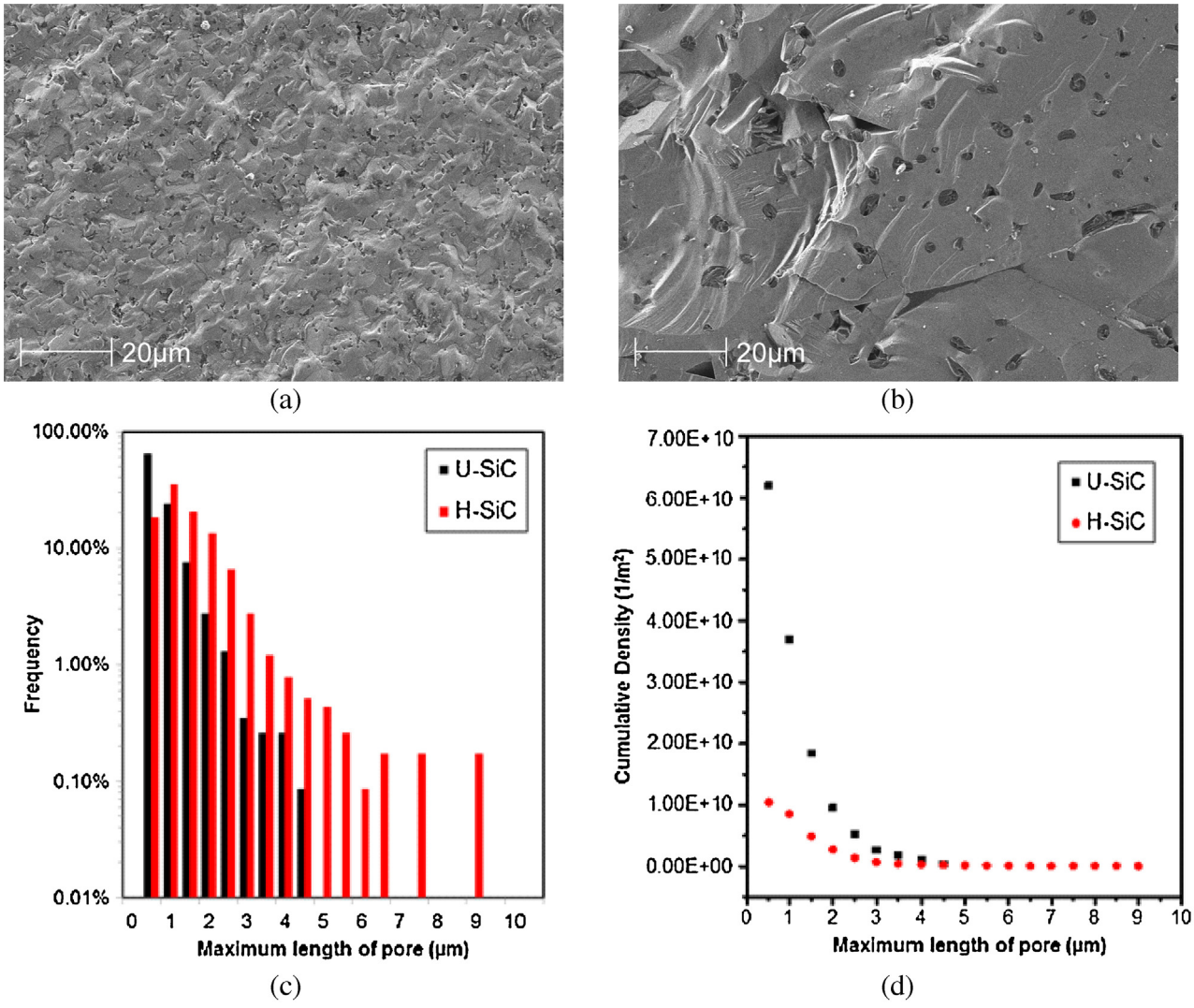

Fig. 9. SEM images detailing the location, shape, size and distribution of pores over the fracture surfaces of (a) U-SiC and (b) H-SiC; (c) histogram of maximum length of pores; (d) cumulative density of pores.

have a finite impact on the nucleation of non-diagonal radial cracks. This is possibly due to the limited propagation caused by the hydrostatic pressure inside the plastic/elastic boundary which can significantly reduce the K around the crack tip, so long as the flaws are sitting on the plastic/elastic boundary and smaller than a threshold value, c^0. However, for pre-existing flaws larger than c^0, the hydrostatic pressure has less of an effect on the K around the crack tip and thus, longer crack growth is expected when cracking is initiated from such larger flaws, particularly when the indentation load become relatively larger.

The fact that H-SiC possesses a higher measured density of larger flaws is agreeable with the generation of more radial cracks along the non-diagonal directions around the Vickers impression. Accordingly, H-SiC may promote the multiplication mechanism by having flaws large enough to have a stress intensity, K, which surpasses the K_C significantly around the elastic/plastic boundary of indentation impression, which leads to a significant propagation before the K drops to a level lower than K_C.

Having seen the difference in the flaw population between U-SiC and H-SiC, we believe that among the microstructural factors, such flaws may originate from the intrinsic pores in each SiC ceramic, rather than being introduced by the grain structure, or, the final polish by 1 μm diamond grits, as supported by Roberts' analysis which dictates that "*the cracks are likely to be of depths comparable to, and in most cases slightly less than, the diameter of the abrasive particles*".[27]

3.6. Porosity

In examining the microstructure, an obvious feature is the residual pores embedded in both SiC ceramics. A measured density of ~3.02 g/cm^3 for U-SiC and ~3.08 g/cm^3 for H-SiC directly corresponds to a calculated porosity of 5.92% and 4.05%. Representative SEM images of fracture surfaces, shown in Fig. 9, depict the location, shape, size and distribution of such pores. In U-SiC, the majority of pores exist on grain boundaries or at triple junctions, whilst in H-SiC they are mostly situated within the grains themselves. Both samples appear to be

dominated by single pores of near-spherical form with a few pore clusters of large, irregular or elongated shape. Given the location of pores in H-SiC, the scale and frequency with which these clusters gather is greater. A comprehensive analysis of the size distribution of pores is provided in the adjoining histograms in Fig. 9(c). For pores with a maximum measured length of <1 μm, the amount present is approximately three times higher in U-SiC than in H-SiC. In contrast, for pores with a maximum measured length >1 μm, H-SiC exceeds that of U-SiC and significantly large pores, from 5 to 9 μm in size, are found to be exclusive to H-SiC. Based on the standard statistic distribution of pore size, one might expect that, if additional areas were to be examined, even bigger pores could be seen, particularly in H-SiC. The cumulative densities of the pores are presented in Fig. 9(d) as a function of flaw size. Up to a size of 4 μm, the accumulative density in U-SiC is generally a few times larger than that in H-SiC. However, despite no pore >4.5 μm being detected, the trend shows that pore densities for sizes beyond 4.5 μm are likely larger in H-SiC compared to U-SiC.

The consistency of the trends observed in flaw population and porosity measurements leads us to conclude that the porosity in these SiC ceramics is a major source of flaws. This is despite the measured flaw density being one order of magnitude smaller than the density of pores. Incidentally, it is possible that the orientation of the flaws on the surface could be responsible for the scale factor difference. The Warren model adopted in order to quantify the surface flaw population assumes that flaws are of a half-penny shape and exactly perpendicular to the tensile stress along the radial direction. In reality, flaws are always randomly oriented. Under such conditions, Warren estimated that the density of surface flaws could be 10× greater in value.[10] Therefore, we propose that the surface flaw densities detected by Hertzian indentation are close enough to the porosity density measurements, particularly in the small size regime, that they are related. In the larger size regime, apart from the large pores that may already be inherent, the coalescence of pores to form pore clusters could likewise act as a large flaw.

4. Summary

The experimental measurements have demonstrated that, despite an almost negligible difference in hardness between the two sintered SiC ceramics tested, a frequently quoted measurement of contact damage resistance, the one with a heterogeneous grain structure displayed a degree of cracking 77.3% higher than that of homogenous SiC. Such a difference in the amount of cracking around the contact of a sharp indenter is primarily due to the difference of pore population, rather than the cracking-resistance or fracture toughness between the two silicon carbides. This conclusion is supported by the following findings:

(a) The grain structure has no effect on the K_{IC} of SiC ceramics measured by Hertzian indention. The recorded improvement in the cracking-resistance measured by VIF is associated with the multiplication of radial cracks around the indentation impression, rather than the cracking-bridging or crack-deflection mechanisms observed in similar SiC ceramics which experience intergranular fracture.[2] This conclusion supports Quinn and Bradt's argument that fracture toughness measured by VIF can be complicated by events occurring around the indenter.

(b) Quantitative measurements of flaw populations revealed that heterogeneous SiC did contain a higher density of large flaws and the largest flaws detected. By analysing the microstructures, it was found that the population of pre-exiting flaws in the SiC ceramics was a reflection of the residual pores retained after sintering. Consequently, it was found that the post-sintering heat treatment not only enhanced the heterogeneity of the grains, both in size and aspect ratio, but also facilitated an increase the density of large pores and thus, is influential in the degree of cracking that occurs around sharp-contact indentations.

Acknowledgements

We gratefully acknowledge the support of the EPSRC-DSTL programme on Enhancing Damage Tolerance through Materials Science under grant EP/G042675/1 and the Scholarship of Loughborough University Graduate School for JW's PhD study. We would also like to thank Prof. Peter Brown from DSTL, Dr Chris Spacie from Morgan AM&T, and all researchers from both Loughborough University and University of Oxford in the UNICAM project for helpful discussion.

References

1. Lee SK, Kim CH. Effect of α-SiC versus β-SiC starting powders on the microstructure and fracture toughness of SiC sintered with Al_2O_3–Y_2O_3 additives. *J Am Ceram Soc* 1994;**77**:1655–8.
2. Padture NP. In situ-toughened silicon carbide. *J Am Ceram Soc* 1994;**77**:519–23.
3. Kim Y-W, Mitomo M, Hirotsuru H. Grain growth and fracture toughness of fine-grained silicon carbide ceramics. *J Am Ceram Soc* 1995;**78**:3145–8.
4. Omari M, Takei H. Pressureless sintering of SiC. *J Am Ceram Soc* 1982;**65**. C-92.
5. Cutler RA, Jackson TB. Liquid phase sintered silicon carbide. In: Tennery VJ, editor. *Ceramic materials and components for engines, proceedings of the third international symposium*. Westerville, OH: The American Ceramic Society; 1989. p. 309–18.
6. Li H, Bradt RC. The effect of indentation-induced cracking on the apparent microhardness. *J Mater Sci* 1996;**31**:1065–70.
7. Quinn G, Green P, Xu K. Cracking and the indentation size effect for Knoop hardness of glasses. *J Am Ceram Soc* 2003;**86**:441–8.
8. Li H, Bradt R. The indentation load/size effect and the measurement of the hardness of vitreous silica. *J Non-Cryst Solids* 1992;**146**:197–212.
9. Rice RW, Wu CC, Borchelt F. Hardness-grain-size relations in ceramics. *J Am Ceram Soc* 1994;**77**:2539–53.
10. Warren PD. Statistical determination of surface flaw distributions in brittle materials. *J Eur Ceram Soc* 1995;**15**:385–94.
11. Medvedovski E. Silicon carbide-based ceramics for ballistic protection. In: Medvedovski E, editor. *Ceramic armor and armor systems*. Westerville, OH: The American Ceramic Society; 2003. p. 19–36.
12. Nader M, Aldinger F, Hoffman MJ. Influence of the α/β-SiC phase transformation on microstructural development and mechanical properties of liquid phase sintered silicon carbide. *J Mater Sci* 1999;**34**:1197–204.

13. Morrel R. Fracture toughness testing for advanced technical ceramics: internationally agreed good practice. *Adv Appl Ceram* 2006;**105**:1–11.
14. Quinn GD, Bradt RC. On the Vickers indentation fracture toughness test. *J Am Ceram Soc* 2007;**90**:673–80.
15. Warren PD. Determining the fracture toughness of brittle materials by Hertzian indentation. *J Eur Ceram Soc* 1995;**15**:201–7.
16. Meyer E. Untersuchungen über Harteprufung und Harte. *Z Phys* 1908;**9**:66–74.
17. Swain M, Wittling M. In: Bradt RC, Hasselman DPH, Munz D, Sakai M, Shevchenko VY, editors. *Indentation size effect for ceramics: is there a fracture mechanics explanation? Fracture mechanics of ceramics*. New York: Plenum; 1996. p. 379–87.
18. Quinn JB, Quinn GD. Indentation brittleness of ceramics: a fresh approach. *J Mater Sci* 1997;**32**:4331–46.
19. Anstis GR, Chantikul P, Lawn BR, Marshall DB. A critical evaluation of indentation techniques for measuring fracture toughness. I. Direct crack measurements. *J Am Ceram Soc* 1981;**64**:533–8.
20. Gilbert CJ, Cao JJ, De Jonghe LC, Ritchie RO. Crack-growth resistance-curve behavior in silicon carbide small versus long cracks. *J Am Ceram Soc* 1997;**80**:2253–61.
21. Padture NP, Lawn BR. Toughness properties of a silicon carbide with an in situ induced heterogeneous grain structure. *J Am Ceram Soc* 1994;**77**:2518–22.
22. Flinders M, Ray D, Anderson A, Cutler RA. High-toughness silicon carbide as armor. *J Am Ceram Soc* 2005;**88**:2217–26.
23. Mulla MA, Krstic VD. Mechanical properties of β-SiC pressureless sintered with Al_2O_3 additions. *Acta Metall Mater* 1994;**1**:303–8.
24. Warren PD, Kolosov OV, Roberts SG, Briggs GAD. Characterization of surface damage via contact probes. *Nanotechnology* 1996;**7**:288–94.
25. Roberts SG, Lawrence CW, Bisrat Y, Warren PD, Hills DA. Determination of surface residual stresses in brittle materials by Hertzian indentation: theory and experiment. *J Am Ceram Soc* 1999;**82**:1809–16.
26. Lawn BR, Evans AG. A model for crack initiation in elastic/plastic indentation fields. *J Mater Sci* 1977;**12**:2195–9.
27. Roberts SG. Depths of cracks produced by abrasion of brittle materials. *Scripta Mater* 1999;**40**:101–8.